Room-Temperature Doping of CsPbBr3 Nanocrystals with Aluminum

Tuan Duong, Dmitry Aldakov, Stéphanie Pouget, Wai-Li Ling, Le Si Dang, Gilles Nogues, Peter Reiss

Room-temperature Doping of $CsPbBr_3$ Nanocrystals with Aluminum

Tuan M. Duong,[1] Dmitry Aldakov,[1] Stéphanie Pouget,[2] Wai Li Ling,[3] Le Si Dang,[4] Gilles Nogues,[4] Peter Reiss[1,*]

[1] Univ. Grenoble Alpes, CEA, CNRS, IRIG, SyMMES, STEP, 38000 Grenoble, France

[2] Univ. Grenoble Alpes, CEA, IRIG, MEM, SGX, 38000 Grenoble, France

[3] Univ. Grenoble Alpes, CEA, CNRS, IBS, 38000 Grenoble, France

[4] Univ. Grenoble Alpes, CNRS, Institut Néel, 38000 Grenoble, France

*Corresponding author email: peter.reiss@cea.fr

Abstract: B-site doping is an emerging strategy for tuning the emission wavelength of cesium lead halide ABX_3 nanocrystals. We present a simple method for the post-synthetic doping of $CsPbBr_3$ nanocrystals with aluminum at room temperature by exposing them to a solution of $AlBr_3$ in dibromomethane. Despite the much smaller ionic radius of Al^{3+} compared to Pb^{2+}, nominal doping levels in a range from 8.1% to 24.3% were obtained when increasing the Al/Pb feed ratio from 1 to 4.5. Al^{3+} introduction leads to a hypsochromic shift of the photoluminescence (PL) emission of the $CsPbBr_3$ nanocrystals. The PL peak position is highly stable over at least 6 months and tunable in a range of 510 to 480 nm by increasing the doping level. Structural analyses revealed a linear correlation between the PL energy and the lattice parameter with a slope of -1.96 eV/Å.

TOC graphics:

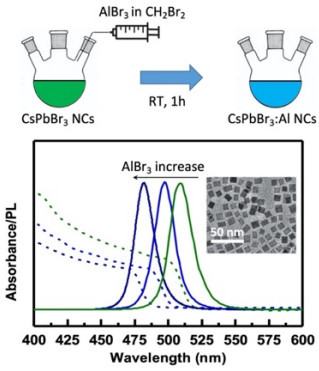

Keywords: metal halide perovskite nanocrystals, doping, photoluminescence, lattice parameter

The most common way of tuning the emission wavelength of lead halide perovskite (ABX_3) nanocrystals (NCs) is by varying the halide composition.[1-3] However, mixed halide perovskites ($ABCl_{1-x}Br_x$, $ABBr_{1-x}I_x$) tend to segregate into the individual single-halide components ($ABCl_3$, $ABBr_3$, ABI_3) under illumination or applied electrical current due to halide migration within the ionic lattice.[4-6] Although this process can be reversed in the dark, it strongly limits the applicability of mixed halide perovskite NCs in light-emitting devices.[7] Cation doping of halide perovskite NCs represents a potential alternative strategy to achieve tunable and stable photoluminescence (PL).[8,9] As an example, Mn^{2+}-doping of $CsPbBr_3$ NCs induces a new emission band due to the intrinsic electronic transition of the dopant ions and can also improve the PL efficiency and photostability.[10,11] Aside from Mn^{2+}, other divalent metal cations have been explored, such as Cd^{2+}, $Zn^{2+,}$ and Sn^{2+},[12,13] which led to a blue (hypsochromic) shift of the emission wavelength and maximum achievable doping levels for the method reported of 16 at% (Cd^{2+}), 10 at% (Sn^{2+}), and 5 at% (Zn^{2+}).[13] Finally, doping of perovskite NCs with *trivalent* ions has been investigated.[14-16] In this case, when Pb^{2+} and the dopant ions share similar sizes, the optical properties are mostly affected by the extra charge from the dopant. While Bi^{3+} generates trap states deeper below the conduction band, reducing the PLQY with increasing dopant

concentration,[15,17] Ce^{3+} creates shallow defects of radiative nature, which can lead to QY enhancement.[14,18] In contrast to these examples, Al^{3+} is a trivalent ion with a significantly smaller size (54 pm) than Pb^{2+} (119 pm). Nonetheless, Al^{3+} could be successfully doped into $CsPbBr_3$ NCs by adding $AlBr_3$ to the reaction precursors at the beginning of the synthesis.[19] Once again a hypsochromic shift of the absorption and emission spectra was observed, which was attributed to a change in the electronic structure of the doped NCs. Theoretical calculations indicated the widening of the bandgap when Al^{3+} was introduced into the host lattice, with only a minor contribution of crystal lattice contraction. Here, we devise a novel and fast method for the post-synthetic room-temperature doping of $CsPbBr_3$ NCs with Al^{3+} giving access to a wide range of doping levels. Furthermore, we correlate doping-induced changes in the lattice parameter with the PL emission energy, revealing a linear relationship with the opposite sign of the slope than that observed in bulk $CsPbBr_3$, i.e., increase of the PL energy with decreasing lattice parameter.

Post-synthetic doping is a convenient way to tune the properties of perovskite NCs without complicating the synthesis reaction by the addition of dopant precursors. The method we developed here for aluminum doping is particularly simple: it consists of the dropwise addition of the dopant precursor solution ($AlBr_3$ in CH_2Br_2) at room temperature within 1 h. As will be discussed below, the choice of dibromomethane as the solvent is of crucial importance for the successful doping process. **Fig. 1** and **Fig. S1** show TEM images of doped and undoped $CsPbBr_3$ NCs. Up to an Al/Pb input ratio of 4.5 a small size increase was observed without affecting the size distribution, namely, for the ratio of 4.5 from 7.6 ± 1.2 nm (**Fig. 1**, undoped sample) to 9.4 ± 1.1 nm (**Fig. 1**, doped sample). For larger Al/Pb ratios the NC size slightly decreased. Moreover, the organization of the NCs on the TEM grid became less ordered, suggesting that the surface of these NCs has been altered.

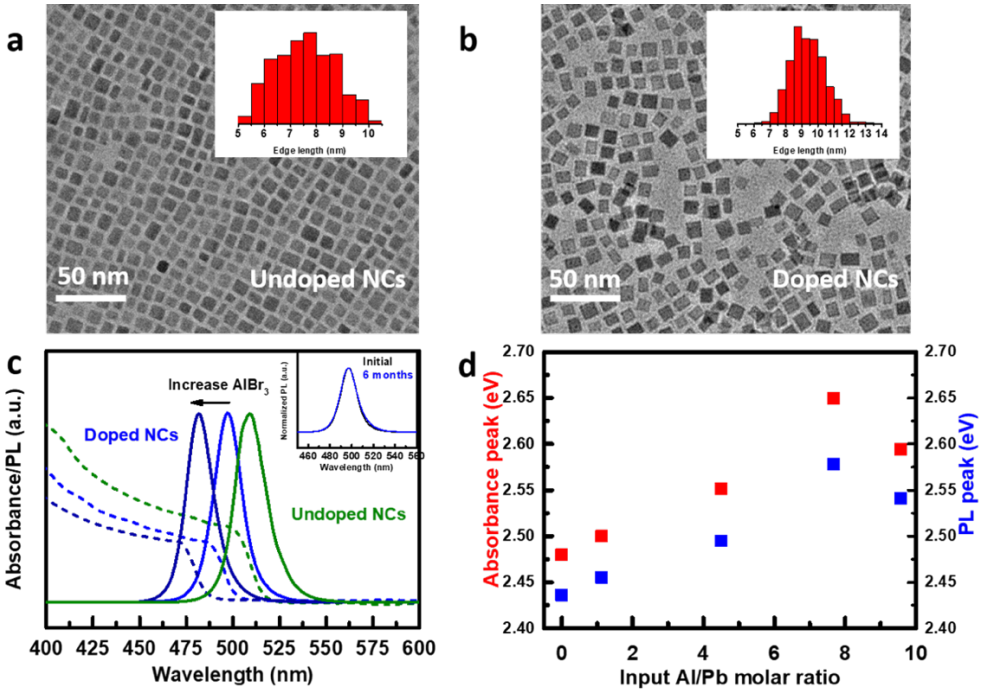

Figure 1. (a), (b) TEM images of the undoped and doped NCs (Al/Pb ratio: 4.5). (c) Absorption and PL spectra of undoped and doped NCs (Al/Pb ratio of 4.5 and 7.7), the inset showing the PL of doped NCs (Al/Pb ratio 4.5) recorded directly after synthesis and after 6 months. (d) Variation in absorption and PL peaks with the doping input ratio.

As visible in **Fig. 1c**, the UV-vis absorption and photoluminescence (PL) spectra exhibited a hypsochromic shift after introducing Al^{3+} and by varying the concentration of the $AlBr_3$ precursor, the PL peak of the doped NCs could be adjusted in a range of 509–482 nm. The photoluminescence quantum yield (PLQY) slightly decreased upon doping from 72.5% for the undoped NCs to 57.4% and 63.5% for the doped sample with an Al/Pb ratio of 4.5 and 7.5, respectively. This decrease is attributed to the additional washing step of the doped samples.[20] Importantly, for a given doping level no spectral shift was observed even after 6 months of storage (**Fig. 1c** inset), which implies that the doping process led to a stable structural configuration. Increasing the Al/Pb input ratio above 8 resulted in a reverse spectral behavior, *i.e.*, a bathochromic shift in both the absorption and PL emission spectra. A similar trend has been observed for the doping of $CsPbBr_3$ NCs with the divalent cations Sn^{2+}, $Cd^{2+,}$ and Zn^{2+}.[13]

Determining the Al^{3+} content with EDX spectroscopy turned out challenging, as the Kα energy of Al (1.4867 keV) is very close to the Lα energy of Br (1.4804 keV), rendering them indistinguishable. Moreover, increasing the incident energy to record the Kα energy of Br (11.9242) presents a significant risk of destroying the sample. Therefore, XPS and ICP-AES were employed to analyze the doped NCs in more detail. In **Fig. 2**, it can be seen that after the post-synthetic treatment with the $AlBr_3/CH_2Br_2$ solution, a new signal related to Al2p was detected at 74.2 eV, corresponding to the Al^{3+} oxidation state. ICP-AES measurements yielded an Al concentration of 8.1%, 15.2%, and 24.3% of Pb when the input Al/Pb ratios were 1, 2.5, and 4.5. Therefore, here the term "doping" is not appropriate *stricto sensu*, as it is generally applied for dopant concentrations in the low percent or sub-percent range. It is noteworthy that the same doping procedure but with the aluminum precursor ($AlBr_3$) dissolved in toluene instead of dibromomethane resulted in no Al^{3+} signal (cf. **Fig. 2b**). In this case, no spectral shifts were observed either, demonstrating that the doping process was unsuccessful. We hypothesize that this difference is due to the molecular structure of $AlBr_3$. In the solid-state, $AlBr_3$ molecules exist as the dimer Al_2Br_6 (**Fig. 2b, inset**). When these molecules are dissolved in aromatic solvents such as benzene or toluene, they retain their dimeric structure.[21] The steric hindrance as well as the coordination sphere of Al_2Br_6 make it unfavorable for Al^{3+} ions to be incorporated into the perovskite structure. In contrast, when CH_2Br_2 is used as the solvent, due to the strong nucleophilicity of the bromide group, it can coordinate more easily with Al_2Br_6, and possibly dissociate the dimer into the $AlBr_3$ monomer or $AlBr_4^-$ ion, both of which can be inserted more easily into the host lattice. Although no direct reference for CH_2Br_2 was found, molecular weight determination and conductivity measurements of $AlBr_3$ dissolved in similar solvents (C_2H_5Br or CH_3Br) agree with this hypothesis.[21,22]

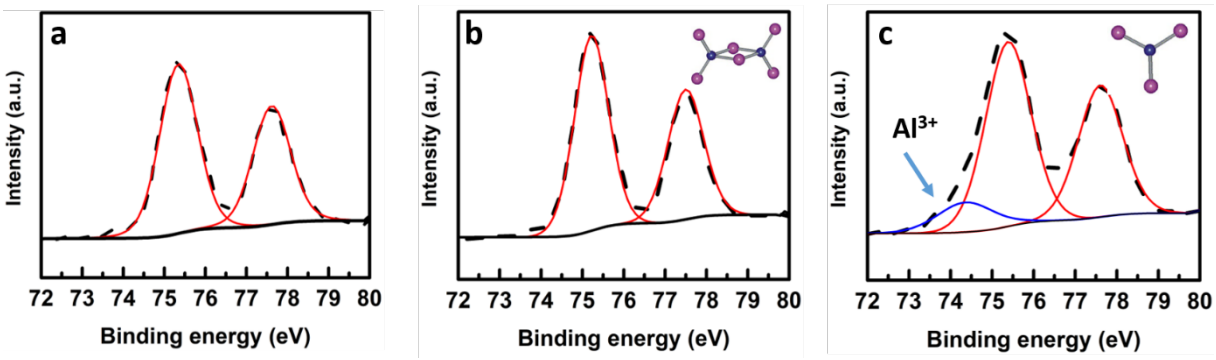

Figure 2. Cs4d XPS spectra of (a) undoped $CsPbBr_3$ NCs, and doped NCs (Al/Pb input ratio: 2.5) using (b) $AlBr_3$/toluene and (c) $AlBr_3/CH_2Br_2$ solutions for the doping process.

There are currently two explanations for the hypsochromic shift of the PL peak upon B-site doping in $CsPbBr_3$ NCs. For divalent cations such as Cd^{2+}, Sn^{2+}, and Zn^{2+}, de Mello Donegá and coworkers reported that doping created strain in the crystal lattice, as shown by the reduced lattice parameter of the doped NCs extracted from HAADF STEM analyses.[13] However, the effect of dopants with other valence states was not investigated. Conversely, for doping with Al^{3+}, Liu et al. proposed that the substitution of Pb^{2+} with Al^{3+} extended the bandgap of the material and introduced a new level within the bandgap.[19] The role of lattice contraction did not play a predominant role in this scenario for explaining the observed spectral shifts.

To elucidate this point in our case, powder X-ray diffraction on a series of samples with different doping levels was performed (Fig. 3). **Fig. 3a** evidences the differences in the relative diffraction peak intensities between the undoped and doped samples. Due to their shape, $CsPbBr_3$ NCs are known to adopt a preferential orientation when deposited on a flat surface. The hypothesis of an altered surface for the doped NCs suggested from TEM observations can explain different degrees of preferential orientation for the different samples, leading to differences in the relative diffraction peak intensities. This was confirmed by X-ray diffraction measurements performed in capillary configuration (cf. **Fig. S5**), which is known to favor random orientation of the crystallites, where the relative peak intensities are coherent with the reference pattern. As expected, compared to the undoped NCs, the diffraction peaks of the doped NCs (Al/Pb input ratio: 4.5) showed a shift to higher angles (**Fig. 3a**).

Since the ionic radius of Al^{3+} is significantly smaller than Pb^{2+}, this shift can be a sign of the lattice contraction induced by the substitution of Pb^{2+} with Al^{3+}. At a first glance, the XRD patterns of both the undoped and doped NCs correspond to that of $CsPbBr_3$ in the cubic phase (ICDD #00-054-0752) (**Fig. 3b**). However, two weak signals at 23° and 28.5° are visible, which can be assigned to the diffraction of the (120) and (122) planes of the $CsPbBr_3$ orthorhombic phase (ICDD #04-014-9676) (**Fig. S3**). While the reported phase of $CsPbBr_3$ NCs at room temperature is indeed orthorhombic,[23] we chose considering the cubic structure which accounts for the main features of the diffraction pattern and leads to better precision in the determination of the lattice parameters by Le Bail refinement (**Fig. 3c and d**). The calculated patterns fitted well with the measured diffraction patterns for both the doped and undoped NCs showing only slight mismatches at 15° and 30.4° due to the use of the cubic structure instead of the orthorhombic one for the refinement. The refined lattice parameter of the undoped NCs is 5.84 Å, which decreases to 5.81 Å upon doping with an Al/Pb input ratio of 4.5. As the amount of dopant was increased, the lattice contraction increased accordingly.

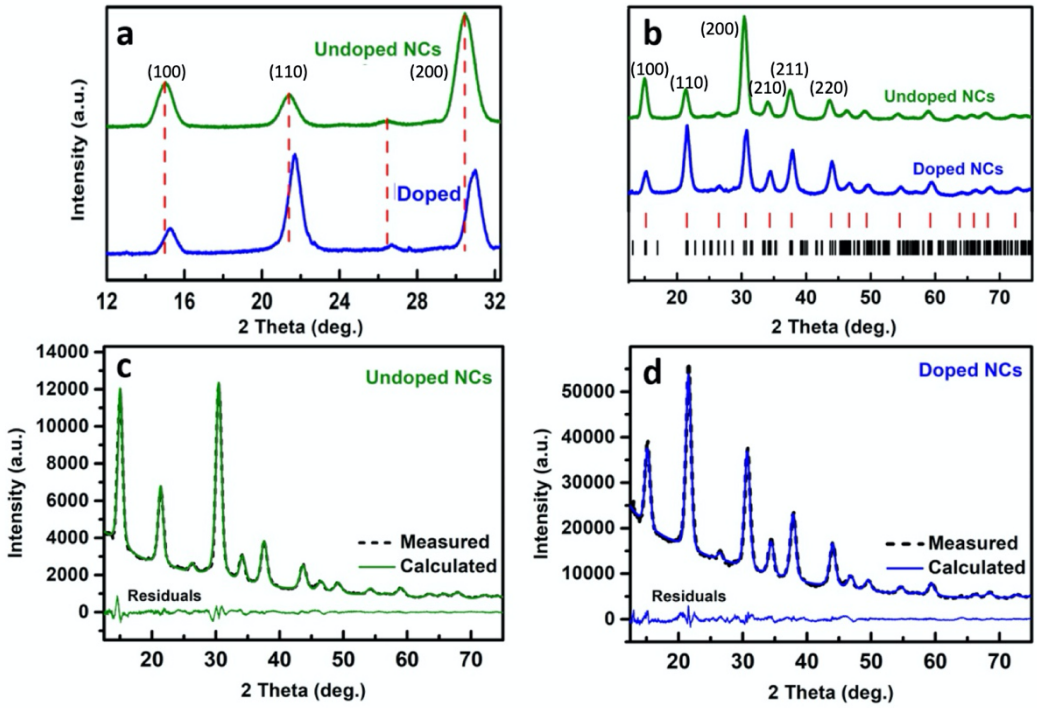

Figure 3. (a) Zoom into the X-ray diffractograms of doped and undoped $CsPbBr_3$ NCs highlighting the shift of the diffraction peaks upon Al^{3+} doping (Al/Pb input ratio: 4.5). (b) XRD patterns of the doped

and undoped NCs, the red and black bars indicate the peak positions of the cubic and orthorhombic reference patterns, respectively. (c) / (d) Le Bail refinement of the cubic structure for the undoped (c) and doped (d) NCs.

Using the data from the Le Bail refinement of samples with different doping levels, we constructed a relationship between the PL peak energy and the lattice parameter (**Fig. 4a**). The fitted line shows an inverse linear relationship between the lattice parameter and the PL peak energy. This trend is similar to that reported in the study of de Mello Donegá et al.,[13] however, with different slopes of -1.96 eV/Å (this work) and -1.61 eV/Å (Ref. 11). The apparent discrepancy in the lattice parameters of samples with similar PL energy is due to the different experimental methods used: while in this work the lattice parameters were extracted from X-ray diffraction, the literature study used electron diffraction. The observed lattice contraction with Al^{3+} (0.55%, ionic radius 54 pm, Al/Pb input ratio of 4.5) is similar to that in Ref. 11 for Cd^{2+} (0.5%, ionic radius 95 pm), albeit smaller than that for Zn^{2+} (0.7%, ionic radius 74 pm). In comparison with the divalent cations used at similar nominal doping levels, Al^{3+} thus induces a lower lattice contraction than expected given its small ionic radius.

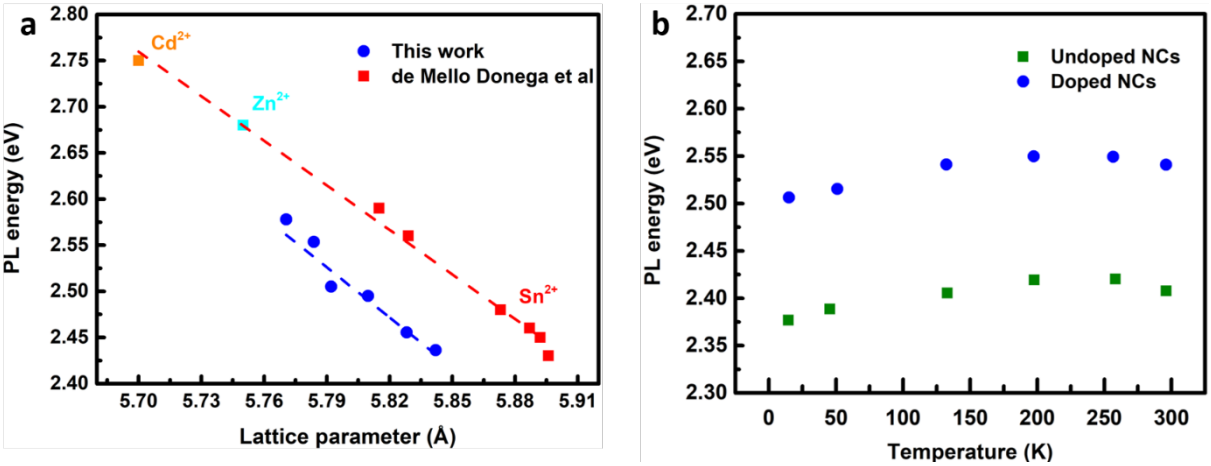

Figure 4. (a) PL peak position as a function of the lattice parameter for NCs doped with Al^{3+} and with divalent dopants (adapted from Fig. 6, Ref. 11). (b) Temperature dependence of the PL peak position of undoped and doped NCs (Al/Pb input ratio: 4.5).

The observed correlation between emission energy and lattice constant, although in line with Ref. 11, stands out against other literature reports.[24-26] Unlike conventional NCs of II-VI or III-V compounds, in lead halide perovskite NCs both band edges are composed of antibonding orbitals.[27,28] When the lattice contracts, we have shrinkage of the Pb–Br bond length, hence stronger antibonding coupling between Pb-6p and Br-4s orbitals for the conduction band minimum (CBM) and between Pb-6s and Br-4p orbitals for the valence band maximum (VBM). Therefore, both CBM and VBM will shift to higher energies. However, the CBM shift is much weaker due to negligible Br-4s hybridization with Pb-6p, so that the overall bandgap becomes narrower and a bathochromic shift of the PL peak is observed when the lattice parameter decreases, e.g., through temperature decrease.[24-26,29] In our case, this behavior is indeed observed for temperatures below approximately 200 K (**Fig. 4b**). Yet there is a change in the slope, and when decreasing the temperature in the range from 300 to 200 K, the PL energy first *increases*. Intriguingly, the doped NCs follow the same trend as the undoped NCs, with the PL energy difference between both samples remaining essentially constant across the whole investigated temperature range. Boziki *et al*. demonstrated that in $CsPbBr_3$ nanocrystals a large distribution of Cs–Pb distances exists in a broad temperature range, which means that the crystalline environment is not uniform, inducing a distribution of band gap values due to deformation and octahedra tilting.[30] Coming back to the origin of the spectral shifts observed upon doping (cf. **Fig. 1 c/d**), the replacement of Pb with significantly smaller Al ions not only produces local lattice shrinkage but also octahedron tilting with respect to the octahedra network. Studies of pressure effects on perovskites have clearly shown that the bandgap increase related to tilting is dominant over the decrease due to lattice shrinkage.[31,32] Hence this effect explains the bandgap increase observed here in the cases of Al-doping and lowering of the temperature in the 300-200 K range.

Concluding, we successfully doped $CsPbBr_3$ NCs with Al^{3+} ions using a facile post-synthetic treatment at room temperature implying $AlBr_3$ dissolved in dibromomethane. The doped NCs exhibited a hypsochromic shift in the absorption and PL spectra, which is tunable with the Al^{3+} dopant concentration and stable over time. Le Bail refinement evidenced a lattice contraction when the

dopant was introduced into the $CsPbBr_3$ host lattice and revealed a linear relationship between the PL energy (and hence bandgap of the NCs) and the lattice parameter with a slope of -1.96 eV/Å. This behavior is opposed to the established relationship between bandgap and lattice parameters for perovskite NCs. Therefore, additional effects such as octahedral tilting and structural disorder need to be considered for explaining the spectral shifts of $CsPbBr_3$ NCs observed upon Al^{3+} doping.

Experimental Methods

$CsPbBr_3$ NC synthesis followed the three-precursor method reported by Imran *et al.*[33] For the Al-doping, 5 mL of a 0.68 µM colloidal solution of $CsPbBr_3$ NCs in toluene were put into a 50 mL reaction flask under Ar flow and stirring. 10-80 µL of $AlBr_3/CH_2Br_2$ solution (1M, Sigma-Aldrich) were diluted in 2 mL of toluene before adding it dropwise within 1 h to the NC colloidal solution using a syringe pump. Finally, the reaction mixture was precipitated with 10 mL of extra dry methyl acetate (ACROS Organics), centrifuged at 10,000 rpm for 5 min, and redispersed in 5 mL of toluene.

Acknowledgment

The authors acknowledge the European Union's Horizon 2020 research and innovation program under the Marie Skłodowska-Curie grant agreement No 754303, which provides the PhD funding for T.M.D, as well as the LABEX Lanef in Grenoble (ANR-10-LABX-51-01) for its support.

Supporting Information: Additional experimental details concerning NC synthesis and characterization, TEM images of samples with different doping levels, the relationship between the input and measured Al/Pb ratio, zoomed-in XRD patterns of the doped and undoped NCs, Pb 4f and Br 3d XPS spectra, and XRD data obtained in capillary configuration.

References

(1) Protesescu, L.; Yakunin, S.; Bodnarchuk, M. I.; Krieg, F.; Caputo, R.; Hendon, C. H.; Yang, R. X.; Walsh, A.; Kovalenko, M. V. Nanocrystals of Cesium Lead Halide Perovskites (CsPbX(3), X = Cl, Br, and I): Novel Optoelectronic Materials Showing Bright Emission with Wide Color Gamut. *Nano Lett.* **2015,** *15*, 3692-3696.

(2) Akkerman, Q. A.; D'Innocenzo, V.; Accornero, S.; Scarpellini, A.; Petrozza, A.; Prato, M.; Manna, L. Tuning the Optical Properties of Cesium Lead Halide Perovskite Nanocrystals by Anion Exchange Reactions. *J. Am. Chem. Soc.* **2015,** *137*, 10276-10281.

(3) Thapa, S.; Bhardwaj, K.; Basel, S.; Pradhan, S.; Eling, C. J.; Adawi, A. M.; Bouillard, J.-S. G.; Stasiuk, G. J.; Reiss, P.; Pariyar, A.et al. Long-term ambient air-stable cubic $CsPbBr_3$ perovskite quantum dots using molecular bromine. *Nanoscale Advances* **2019,** *1*, 3388-3391.

(4) Braly, I. L.; Stoddard, R. J.; Rajagopal, A.; Uhl, A. R.; Katahara, J. K.; Jen, A. K. Y.; Hillhouse, H. W. Current-Induced Phase Segregation in Mixed Halide Hybrid Perovskites and its Impact on Two-Terminal Tandem Solar Cell Design. *ACS Energy Lett.* **2017,** *2*, 1841-1847.

(5) Duong, T.; Mulmudi, H. K.; Wu, Y.; Fu, X.; Shen, H.; Peng, J.; Wu, N.; Nguyen, H. T.; Macdonald, D.; Lockrey, M.et al. Light and Electrically Induced Phase Segregation and Its Impact on the Stability of Quadruple Cation High Bandgap Perovskite Solar Cells. *ACS Appl. Mater. Interfaces* **2017,** *9*, 26859-26866.

(6) Zhang, H.; Fu, X.; Tang, Y.; Wang, H.; Zhang, C.; Yu, W. W.; Wang, X.; Zhang, Y.; Xiao, M. Phase segregation due to ion migration in all-inorganic mixed-halide perovskite nanocrystals. *Nat. Commun.* **2019,** *10*, 1088.

(7) Knight, A. J.; Herz, L. M. Preventing phase segregation in mixed-halide perovskites: a perspective. *En. Env. Sci.* **2020,** *13*, 2024-2046.

(8) Chen, Y.; Liu, Y.; Hong, M. Cation-doping matters in caesium lead halide perovskite nanocrystals: from physicochemical fundamentals to optoelectronic applications. *Nanoscale* **2020,** *12*, 12228-12248.

(9) Aldakov, D.; Reiss, P. Safer-by-Design Fluorescent Nanocrystals: Metal Halide Perovskites vs Semiconductor Quantum Dots. *J. Phys. Chem. C* **2019,** *123*, 12527-12541.

(10) Mir, W. J.; Swarnkar, A.; Nag, A. Postsynthesis Mn-doping in $CsPbI_3$ nanocrystals to stabilize the black perovskite phase. *Nanoscale* **2019,** *11*, 4278-4286.

(11) Qiao, T.; Parobek, D.; Dong, Y.; Ha, E.; Son, D. H. Photoinduced Mn doping in cesium lead halide perovskite nanocrystals. *Nanoscale* **2019,** *11*, 5247-5253.

(12) Imran, M.; Ramade, J.; Di Stasio, F.; De Franco, M.; Buha, J.; Van Aert, S.; Goldoni, L.; Lauciello, S.; Prato, M.; Infante, I.et al. Alloy $CsCd_xPb_{1-x}Br_3$ Perovskite Nanocrystals: The Role of Surface Passivation in Preserving Composition and Blue Emission. *Chem. Mater.* **2020,** *32*, 10641-10652.

(13) van der Stam, W.; Geuchies, J. J.; Altantzis, T.; van den Bos, K. H. W.; Meeldijk, J. D.; Van Aert, S.; Bals, S.; Vanmaekelbergh, D.; de Mello Donega, C. Highly Emissive Divalent-Ion-Doped Colloidal $CsPb_{1-x}M_xBr_3$ Perovskite Nanocrystals through Cation Exchange. *J. Am. Chem. Soc.* **2017,** *139*, 4087-4097.

(14) Yao, J. S.; Ge, J.; Han, B. N.; Wang, K. H.; Yao, H. B.; Yu, H. L.; Li, J. H.; Zhu, B. S.; Song, J. Z.; Chen, C.et al. Ce(3+)-Doping to Modulate Photoluminescence Kinetics for Efficient $CsPbBr_3$ Nanocrystals Based Light-Emitting Diodes. *J. Am. Chem. Soc.* **2018,** *140*, 3626-3634.

(15) Lozhkina, O. A.; Murashkina, A. A.; Shilovskikh, V. V.; Kapitonov, Y. V.; Ryabchuk, V. K.; Emeline, A. V.; Miyasaka, T. Invalidity of Band-Gap Engineering Concept for Bi(3+) Heterovalent Doping in $CsPbBr_3$ Halide Perovskite. *J. Phys. Chem. Lett.* **2018,** *9*, 5408-5411.

(16) Lu, C.-H.; Biesold-McGee, G. V.; Liu, Y.; Kang, Z.; Lin, Z. Doping and ion substitution in colloidal metal halide perovskite nanocrystals. *Chem. Soc. Rev.* **2020,** *49*, 4953-5007.

(17) Begum, R.; Parida, M. R.; Abdelhady, A. L.; Murali, B.; Alyami, N. M.; Ahmed, G. H.; Hedhili, M. N.; Bakr, O. M.; Mohammed, O. F. Engineering Interfacial Charge Transfer in $CsPbBr_3$ Perovskite Nanocrystals by Heterovalent Doping. *J. Am. Chem. Soc.* **2017,** *139*, 731-737.
(18) Zhou, D.; Liu, D.; Pan, G.; Chen, X.; Li, D.; Xu, W.; Bai, X.; Song, H. Cerium and Ytterbium Codoped Halide Perovskite Quantum Dots: A Novel and Efficient Downconverter for Improving the Performance of Silicon Solar Cells. *Adv. Mater.* **2017,** *29*, 1704149.
(19) Liu, M.; Zhong, G.; Yin, Y.; Miao, J.; Li, K.; Wang, C.; Xu, X.; Shen, C.; Meng, H. Aluminum-Doped Cesium Lead Bromide Perovskite Nanocrystals with Stable Blue Photoluminescence Used for Display Backlight. *Adv. Sci.* **2017,** *4*, 1700335.
(20) Tamayo, J.; Do, T.; El-Maraghy, K.; Vullev, V. I. Are the emission quantum yields of cesium plumbobromide perovskite nanocrystals reliable metrics for their quality? *J. Photochem. Photobiol.* **2022,** *10*, 100109.
(21) Brown, H. C.; Wallace, W. J. Addition Compounds of Aluminum Halides with Alkyl Halides1. *J. Am. Chem. Soc.* **1953,** *75*, 6279-6285.
(22) Grattan, D. W.; Plesch, P. H. Ionisation of aluminium halides in alkyl halides. *J. Chem. Soc., Dalton Trans.* **1977**, *18*, 1734.
(23) Cottingham, P.; Brutchey, R. L. On the crystal structure of colloidally prepared $CsPbBr_3$ quantum dots. *Chem. Commun.* **2016,** *52*, 5246-5249.
(24) Lee, S. M.; Moon, C. J.; Lim, H.; Lee, Y.; Choi, M. Y.; Bang, J. Temperature-Dependent Photoluminescence of Cesium Lead Halide Perovskite Quantum Dots: Splitting of the Photoluminescence Peaks of $CsPbBr_3$ and $CsPb(Br/I)_3$ Quantum Dots at Low Temperature. *J. Phys. Chem. C* **2017,** *121*, 26054-26062.
(25) Cheng, O. H.; Qiao, T.; Sheldon, M.; Son, D. H. Size- and temperature-dependent photoluminescence spectra of strongly confined $CsPbBr_3$ quantum dots. *Nanoscale* **2020,** *12*, 13113-13118.
(26) Shinde, A.; Gahlaut, R.; Mahamuni, S. Low-Temperature Photoluminescence Studies of $CsPbBr_3$ Quantum Dots. *J. Phys. Chem. C* **2017,** *121*, 14872-14878.
(27) Umebayashi, T.; Asai, K.; Kondo, T.; Nakao, A. Electronic structures of lead iodide based low-dimensional crystals. *Phys. Rev. B* **2003,** *67*, 155405.
(28) Butler, K. T.; Frost, J. M.; Walsh, A. Band alignment of the hybrid halide perovskites $CH_3NH_3PbCl_3$, $CH_3NH_3PbBr_3$ and $CH_3NH_3PbI_3$. *Mater. Horizons* **2015,** *2*, 228-231.
(29) Mannino, G.; Deretzis, I.; Smecca, E.; La Magna, A.; Alberti, A.; Ceratti, D.; Cahen, D. Temperature-Dependent Optical Band Gap in $CsPbBr_3$, $MAPbBr_3$, and $FAPbBr_3$ Single Crystals. *J. Phys. Chem. Lett.* **2020,** *11*, 2490-2496.
(30) Boziki, A.; Dar, M. I.; Jacopin, G.; Grätzel, M.; Rothlisberger, U. Molecular Origin of the Asymmetric Photoluminescence Spectra of $CsPbBr_3$ at Low Temperature. *J. Phys. Chem. Lett.* **2021,** *12*, 2699-2704.
(31) Lü, X.; Yang, W.; Jia, Q.; Xu, H. Pressure-induced dramatic changes in organic–inorganic halide perovskites. *Chem. Sci.* **2017,** *8*, 6764-6776.
(32) Wang, L.; Wang, K.; Zou, B. Pressure-Induced Structural and Optical Properties of Organometal Halide Perovskite-Based Formamidinium Lead Bromide. *J. Phys. Chem. Lett.* **2016,** *7*, 2556-2562.
(33) Imran, M.; Caligiuri, V.; Wang, M.; Goldoni, L.; Prato, M.; Krahne, R.; De Trizio, L.; Manna, L. Benzoyl Halides as Alternative Precursors for the Colloidal Synthesis of Lead-Based Halide Perovskite Nanocrystals. *J. Am. Chem. Soc.* **2018,** *140*, 2656-2664.